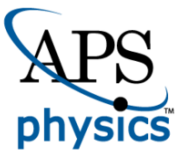

Pairing Correlations across the Superfluid Phase Transition in the Unitary Fermi Gas

S. Jensen, C. N. Gilbreth, and Y. Alhassid

Phys. Rev. Lett. **124**, 090604 — Published 2 March 2020

DOI: 10.1103/PhysRevLett.124.090604

Nature of pairing correlations in the homogeneous Fermi gas at unitarity

S. Jensen,[1] C. N. Gilbreth,[2] and Y. Alhassid[1]
[1] *Center for Theoretical Physics, Sloane Physics Laboratory, Yale University, New Haven, CT 06520*
[2] *Institute for Nuclear Theory, Box 351550, University of Washington, Seattle, WA 98195*

In the two-component Fermi gas with a contact interaction, a pseudogap regime can exist at temperatures between the superfluid critical temperature T_c and a temperature $T^* > T_c$. This regime is characterized by pairing correlations without superfluidity. However, in the unitary limit of infinite scattering length, the existence of this regime is still debated. To help address this, we have applied finite-temperature auxiliary-field quantum Monte Carlo (AFMC) to study the thermodynamics of the superfluid phase transition and signatures of the pseudogap in the spin-balanced homogeneous unitary Fermi gas. We present results at finite filling factor $\nu \simeq 0.06$ for the condensate fraction, an energy-staggering pairing gap, the spin susceptibility, and the heat capacity, and compare them to experimental data when available. In contrast to previous AFMC simulations, our model space consists of the complete first Brillouin zone of the lattice, and our calculations are performed in the canonical ensemble of fixed particle number. The canonical ensemble AFMC framework enables the calculation of a model-independent gap, providing direct information on pairing correlations without the need for numerical analytic continuation. We use finite-size scaling to estimate T_c at the corresponding filling factor. We find that the energy-staggering pairing gap vanishes above T_c, showing no pseudogap effects, and that the spin susceptibility shows a substantially reduced signature of a spin gap compared to previously reported AFMC simulations.

Introduction.— The unitary Fermi gas (UFG) is the infinite-scattering-length limit of a system of spin-1/2 fermions with a zero-range interaction. This system is relevant to a variety of physical systems, including neutron stars, strongly correlated QCD matter [1] and high-T_c superconductors [2]. The homogenous UFG is a strongly correlated quantum many-body system characterized by a single energy scale and is of broad interest as a testing ground for many-body theories.

The UFG has been realized experimentally using ultracold dilute gases of ^{6}Li and ^{40}K; see, e.g., Refs. [3, 4]. These experiments have measured various properties of the UFG, including the thermal energy, pressure, heat capacity, compressibility, and spectral function [5–9]. The UFG exhibits a superfluid phase transition at a critical temperature measured as $T_c = 0.167(13)T_F$ [5] where T_F is the Fermi temperature.

The nature of pairing correlations in the UFG above T_c remains incompletely understood. In particular, a pseudogap regime, in which pairing correlations exist even though a superfluid condensate is not present, was proposed to exist above T_c. Such a regime exists in the BEC limit, where particles pair to form bound dimers at a temperature T^* and condense at the critical temperature $T_c < T^*$. However, in the UFG, it is still debated whether T_c and the temperature scale T^* for pairing should coincide or differ, and if they differ, what the properties of the pseudogap regime $T_c < T < T^*$ are.

A number of experimental works claimed to have observed signatures of a pseudogap in the UFG [9, 10], while others have seen no signatures of a pseudogap [5, 6, 11, 12]. Similar differences emerged in theoretical studies, with some showing a signature of a pseudogap [10, 13–22], and others not [23, 24]. For a recent review, see Ref. [25]. A wide variety of theoretical methods were applied to study the superfluid phase transition of the UFG [26]. While these methods provided important insight into the physics of the UFG, *ab initio* simulations can provide the most accurate results [27–31].

Here we apply finite-temperature auxiliary-field quantum Monte Carlo (AFMC) on a lattice to study the thermodynamic properties of the homogeneous UFG. Our calculations differ from previous AFMC calculations [13, 15, 32] in that (i) we do not use a spherical cutoff in the single-particle momentum space, but include the complete first Brillouin zone, leading to qualitatively different results, (ii) we use the canonical ensemble of fixed particle number, allowing the direct computation of a model-independent pairing gap from the staggering of energy in particle number without the need for numerically difficult analytic continuation, (iii) we extrapolate to zero imaginary time step, and (iv) we calculate the heat capacity, which is challenging to compute in quantum Monte Carlo simulations. We also present results for the condensate fraction and static spin susceptibility.

Our calculations are done for a small but finite filling factor of $\nu \simeq 0.06$. We use finite-size scaling of the condensate fraction to determine a critical temperature of $T_c \simeq 0.130(15)T_F$ at this finite density. We find that the model-independent pairing gap vanishes at temperatures larger than T_c, and thus does not show pseudogap effects, in contrast to the conclusions of Refs. [13, 32]. The spin susceptibility shows a moderate suppression above T_c and below a spin-gap temperature of $T^* \lesssim 0.17\,T_F$, in contrast to the value of $T^* \simeq 0.25\,T_F$ found in Ref. [15].

Extensive supplemental material accompanies this article, in which we discuss important technical details [33].

Lattice formulation and Hamiltonian.— We consider N spin-1/2 fermions that interact via a contact interaction $V = V_0\delta(\mathbf{r} - \mathbf{r}')$ within a spatial volume with periodic

boundary conditions. The volume is discretized into a lattice with an odd number N_L of points in each dimension, each lattice point centered within a cube of side length δx. The lattice Hamiltonian is

$$\hat{H} = \sum_{\mathbf{k},s} \epsilon_{\mathbf{k}} \hat{a}^\dagger_{\mathbf{k},s} \hat{a}_{\mathbf{k},s} + g \sum_{\mathbf{x}} \hat{n}_{\mathbf{x},\uparrow} \hat{n}_{\mathbf{x},\downarrow} \,, \tag{1}$$

where $\hat{a}^\dagger_{\mathbf{k},s}$ and $\hat{a}_{\mathbf{k},s}$ are creation and annihilation operators for fermions with wavevector $\mathbf{k}$ and spin projection $s = \pm 1/2$, and the single-particle dispersion relation is $\epsilon_{\mathbf{k}} = \hbar^2 \mathbf{k}^2/2m$. The coupling constant is $g = V_0/(\delta x)^3$ and $\hat{n}_{\mathbf{x},s} = \hat{\psi}^\dagger_{\mathbf{x},s} \hat{\psi}_{\mathbf{x},s}$, where $\hat{\psi}^\dagger_{\mathbf{x},s}, \hat{\psi}_{\mathbf{x},s}$ obey anticommutation relations $\{\hat{\psi}^\dagger_{\mathbf{x},s}, \hat{\psi}_{\mathbf{x}',s'}\} = \delta_{\mathbf{x},\mathbf{x}'} \delta_{s,s'}$.

Our single-particle model space consists of all single-particle states with spin projection $s = \pm 1/2$ and momentum $\hbar\mathbf{k}$ within the complete first Brillouin zone of the lattice, described by a cube $|k_i| \le k_c$ $(i = x, y, z)$ with $k_c = \pi/\delta x$. The thermodynamic limit of the UFG is recovered in the limits of zero filling factor ($\nu = N/N_L^3 \to 0$) and large number of fermions ($N \to \infty$).

We choose V_0 to reproduce the scattering length a [43]

$$\frac{1}{V_0} = \frac{m}{4\pi\hbar^2 a} - \int_B \frac{d^3k}{(2\pi)^3 2\epsilon_{\mathbf{k}}} \,, \tag{2}$$

which is derived by solving the Lippmann-Schwinger equation. We use the complete first Brillouin zone B when calculating the integral in (2). Solving the scattering problem numerically on the lattice, we find that Eq. (2) is very accurate even for finite lattices: on the 9^3 lattice it yields $a^{-1} = 0.006\,(\delta x)^{-1}$ and an effective range of $r_e = 0.34\,\delta x$ [33], in close agreement with its value $r_e = 0.337\,\delta x$ in the limit of large lattices [43].

Finite-temperature AFMC.— The AFMC method (for a recent review, see Ref. [44]) is based on the Hubbard-Stratonovich (HS) transformation [45, 46], which expresses the thermal propagator $e^{-\beta\hat{H}}$ ($\beta = 1/k_B T$ is the inverse temperature T with Boltzmann constant k_B) as a path integral over external auxiliary fields.

Dividing the imaginary time β into N_τ imaginary times of length $\Delta\beta$, we use a symmetric Trotter decomposition

$$e^{-\beta\hat{H}} = [e^{-\Delta\beta\hat{H}_0/2} e^{-\Delta\beta\hat{V}} e^{-\Delta\beta\hat{H}_0/2}]^{N_\tau} + O((\Delta\beta)^2) \,, \tag{3}$$

where $\hat{H}_0$ and $\hat{V}$ are, respectively, the kinetic energy and interaction terms of the Hamiltonian $\hat{H}$ in Eq. (1). Rewriting the interaction as $\hat{V} = g \sum_{\mathbf{x}} (\hat{n}_{\mathbf{x}}^2 - \hat{n}_{\mathbf{x}})/2$ where $\hat{n}_{\mathbf{x}} = \hat{n}_{\mathbf{x},\uparrow} + \hat{n}_{\mathbf{x},\downarrow}$, and expressing $\exp\left(-\Delta\beta g \hat{n}_{\mathbf{x}}^2/2\right)$ at each of the N_L^3 lattice points $\mathbf{x}$ and N_τ time slices $\tau_n = n\Delta\beta$ $(n = 1, 2, \ldots, N_\tau)$ as a Gaussian integral over an auxiliary field $\sigma_{\mathbf{x}}(\tau_n)$, the propagator becomes

$$e^{-\beta\hat{H}} = \int D[\sigma] G_\sigma \hat{U}_\sigma + O((\Delta\beta)^2) \,. \tag{4}$$

Here $D[\sigma] = \prod_{\mathbf{x},n} \left[d\sigma_{\mathbf{x}}(\tau_n) \sqrt{\Delta\beta |g|/2\pi} \right]$ is the integration measure, $G_\sigma = e^{-\frac{1}{2}|g|\Delta\beta \sum_{\mathbf{x},n} \sigma^2_{\mathbf{x}}(\tau_n)}$, and $\hat{U}_\sigma = \prod_n e^{-\Delta\beta\hat{H}_0/2} e^{-\Delta\beta\hat{h}_\sigma(\tau_n)} e^{-\Delta\beta\hat{H}_0/2}$ (a time-ordered product) with $\hat{h}_\sigma(\tau_n) = g \sum_{\mathbf{x}} \sigma_{\mathbf{x}}(\tau_n) \hat{n}_{\mathbf{x}} - g\hat{N}/2$ is the propagator of non-interacting fermions in time-dependent fields $\sigma_{\mathbf{x}}(\tau)$. We use a fast Fourier transform [13, 15, 32] to efficiently change basis between coordinate and momentum space in order to implement the potential and the quadratic single-particle dispersion relation, respectively. We discretize the integral over each of the σ fields using a three-point Gaussian quadrature [47].

The thermal expectation value of an observable $\hat{O}$ is

$$\langle \hat{O} \rangle = \frac{\mathrm{Tr}(\hat{O} e^{-\beta\hat{H}})}{\mathrm{Tr}(e^{-\beta\hat{H}})} = \frac{\int D[\sigma] \langle \hat{O} \rangle_\sigma W_\sigma \Phi_\sigma}{\int D[\sigma] W_\sigma \Phi_\sigma} \,, \tag{5}$$

where $W_\sigma = G_\sigma |\mathrm{Tr}(\hat{U}_\sigma)|$, $\Phi_\sigma = \mathrm{Tr}(\hat{U}_\sigma)/|\mathrm{Tr}(\hat{U}_\sigma)|$ is the Monte Carlo sign, and $\langle \hat{O} \rangle_\sigma = \mathrm{Tr}(\hat{O}\hat{U}_\sigma)/\mathrm{Tr}(\hat{U}_\sigma)$ is the expectation of $\hat{O}$ with respect to a field configuration σ. In AFMC, we sample uncorrelated field configurations according to the positive-definite weight W_σ and use them to estimate $\langle \hat{O} \rangle$ and its statistical fluctuation.

We project onto fixed particle number N_s for each spin s using the discrete Fourier transform

$$\hat{P}_{N_s} = \frac{e^{-\beta\mu N_s}}{M} \sum_{m=1}^{M} e^{-i\varphi_m N_s} e^{(\beta\mu + i\varphi_m)\hat{N}_s} \,, \tag{6}$$

where $\varphi_m = \frac{2\pi m}{M}$ and $M = N_L^3$. The chemical potential μ in (6), chosen to give approximately an average N_s, ensures the numerical stability of the Fourier sum. The traces in (5) are computed as canonical traces, $\mathrm{Tr}_{N_\uparrow, N_\downarrow} \hat{X} = \mathrm{Tr}(\hat{P}_{N_\uparrow} \hat{P}_{N_\downarrow} \hat{X})$, which are sums of grand-canonical traces using Eq. (6). These grand-canonical traces can be computed using the matrix $\mathbf{U}_\sigma$ that represents $\hat{U}_\sigma$ in the single-particle space, e.g.,

$$\mathrm{Tr}_{\mathrm{GC}}[e^{(\beta\mu + i\varphi_m)\hat{N}} \hat{U}_\sigma] = \det[\mathbb{1} + e^{(\beta\mu + i\varphi_m)} \mathbf{U}_\sigma] \,. \tag{7}$$

We use the diagonalization method of Refs. [48, 49] to compute more efficiently the Fourier sums in the number projection. We also use algorithmic improvements we developed for finite-temperature AFMC calculations of dilute fermionic systems [33, 50] that have enabled our large-lattice simulations.

Results.— We performed AFMC simulations for $N = 20, 40, 80$ and 130 particles on lattices of size $7^3, 9^3, 11^3$ and 13^3, respectively, keeping the filling factor low and constant at $\nu \equiv N/N_L^3 \simeq 0.06$. The ratio of the effective range $r_e \approx 0.337\,\delta x$ [43] to the Fermi wavelength is then $k_{\mathrm{F}} r_e \simeq 0.41$. We use multiple $\Delta\beta$ values for each β and a quadratic fit to extrapolate the observables to $\Delta\beta = 0$. For each run, we collect typically between 3,000 and 30,000 thermalized and uncorrelated samples [33].

(i) Condensate fraction: The existence of off-diagonal long-range order in the two-body density matrix $\langle \hat{\psi}^\dagger_{\mathbf{k}_1,\uparrow} \hat{\psi}^\dagger_{\mathbf{k}_2,\downarrow} \hat{\psi}_{\mathbf{k}_3,\downarrow} \hat{\psi}_{\mathbf{k}_4,\uparrow} \rangle$ is equivalent to this matrix having a large eigenvalue which scales with the system size [51]. We calculated the condensate fraction

n from the largest eigenvalue λ, which satisfies $\lambda \leq N(M-N/2+1)/(2M) \leq N/2$, using the definition

$$n = \langle\lambda\rangle/[N(M-N/2+1)/(2M)]\,, \qquad (8)$$

where $M = N_L^3$ is the number of lattice points. In Fig. 1(a), we show the AFMC condensate fraction for 20, 40, 80, and 130 particles (solid symbols). We compare with the experimental values of Ref. [5] (open circles) and the simulations of Ref. [32] (open squares); for the latter we show the results of the largest lattice reported, 10^3.

To obtain the thermodynamic and continuum limits, one must extrapolate to infinite particle number and zero filling factor $\nu \to 0$ or equivalently $k_F r_e \to 0$ [27, 56, 57]. To determine T_c in the thermodynamic limit at fixed filling factor, we performed a finite-size scaling analysis using the condensate fraction (see Fig. 5 of [33]). We find $T_c \simeq 0.130(15) T_F$ for the filling factor of $\nu \simeq 0.06$, shown by the vertical band in Fig. 1. The Fermi temperature is defined by $T_F = \varepsilon_F/k_B$ where $\varepsilon_F = (\hbar^2/2m)(3\pi^2\rho)^{2/3}$ is the Fermi energy and $\rho = \nu/(\delta x)^3$ is the density. The lower value of T_c at finite filling factor as compared with the experimental value of Ref. [5] is consistent with the findings of Ref. [58] that the finite effective range of the interaction suppresses the attractive pairing correlations. The continuum limit requires further studies with large-lattice simulations. We leave this to future studies.

(ii) Energy-staggering pairing gap: Using the canonical ensemble, we calculated a model-independent thermal energy-staggering pairing gap

$$\Delta_E = [2E(N_\uparrow, N_\downarrow - 1) - E(N_\uparrow, N_\downarrow) - E(N_\uparrow - 1, N_\downarrow - 1)]/2\,. \qquad (9)$$

Here $E(N_\uparrow, N_\downarrow)$ is the thermal energy for a system with $N_\uparrow$ spin-up particles and $N_\downarrow$ spin-down particles. In calculating (9), we used a particle-number reprojection method [48, 59]. This gap does not require a numerical analytic continuation and provides direct information on pairing correlations. At zero temperature, the energy-staggering pairing gap of the UFG was first studied using quantum Monte Carlo in Ref. [60].

The pseudogap scenario suggests that pairing correlations appear below a temperature scale $T^* > T_c$. Such correlations can have various signatures, including a depression in the single-particle density of states, a gap in the single-particle excitation spectrum, and a suppression of the spin susceptibility referred to as "spin-gap" [25]. If pair formation is energetically favorable, the energy-staggering gap Δ_E should be nonzero. However, as shown in Fig. 1(b), Δ_E, which is largely converged on the 13^3 lattice near T_c, vanishes above $T_c \simeq 0.130(15) T_F$ and does not exhibit a pseudogap signature.

A pairing gap of $\simeq 0.35-0.5\,\varepsilon_F$ was reported at $T/T_F = 0.15$ [13, 14] (which is the estimated critical temperature of Ref. [32]) by fitting the AFMC spectral function to a BCS-like dispersion. Those calculations are shown by the open squares in Fig. 1(b). It is unclear whether the gap computed from the spectral function and the gap computed from the energy staggering should agree for the UFG; it would be interesting to perform calculations of these quantities within the same framework.

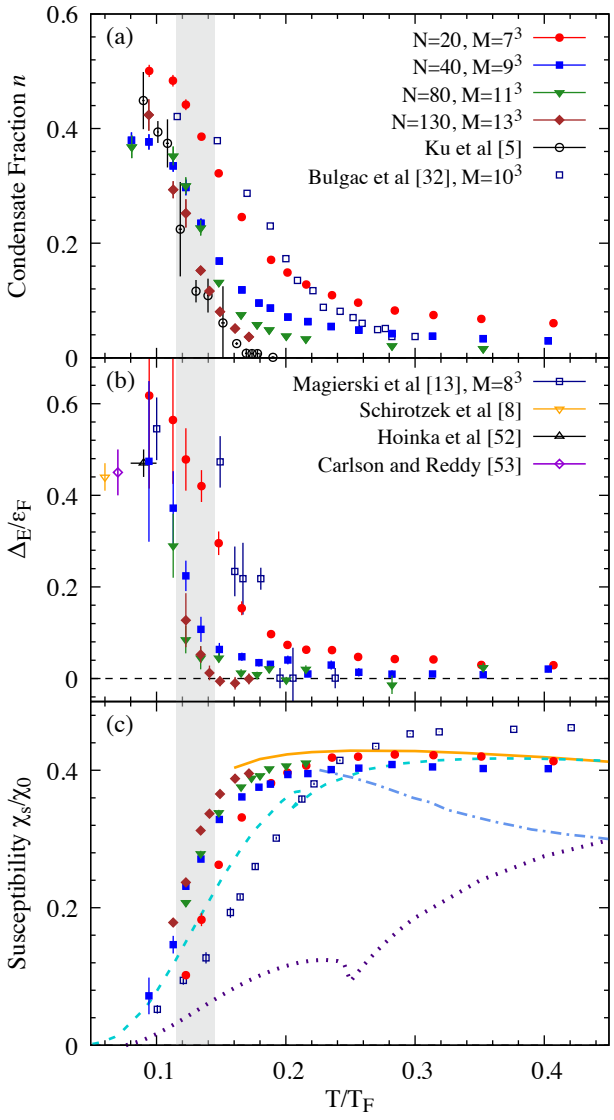

FIG. 1. (a) AFMC condensate fraction n (solid symbols) compared with experiment [5] (open circles) and previous AFMC results [32] (open squares). (b) AFMC energy-staggering pairing gap compared with previous AFMC results [13] (open squares) and the low-temperature experiments of Ref. [52] (open up triangle) and Ref. [8] (open down triangle). We also compare with the $T = 0$ quantum Monte Carlo result of Ref. [53](open diamond). (c) AFMC spin susceptibility compared with the Luttinger-Ward theory [24] (solid line), the previous AFMC results of Ref. [15] (open squares), the t-matrix results of Ref. [20] (dotted line), the extended T-matrix result of Refs. [21, 54] (dashed line), and the self-consistent NSR results of Ref. [55] (dashed-dotted line). The vertical band is our estimate for $T_c \simeq 0.130(15)\,T_F$.

(iii) Spin susceptibility: In the presence of pairing correlations, spin-flip excitations require the breaking of pairs, causing a suppression of the spin susceptibility [19, 61, 62]. The spin susceptibility χ_s is given by

$$\chi_s = \frac{\beta}{V}\langle(\hat{N}_\uparrow - \hat{N}_\downarrow)^2\rangle \,, \tag{10}$$

where the expectation value on the r.h.s. of (10) is calculated for the spin-balanced system $\langle\hat{N}_\uparrow\rangle = \langle\hat{N}_\downarrow\rangle$. We calculated χ_s in AFMC using only one particle-number projection onto the total number of particles $N = N_\uparrow + N_\downarrow$. In Fig. 1(c) we show our results (solid symbols) for χ_s in units of the $T = 0$ free Fermi gas susceptibility $\chi_0 = 3\rho/2\varepsilon_F$. We also compare with the Luttinger-Ward theory of Ref. [24] and the 12^3 lattice AFMC results of Ref. [15] (open squares), the t-matrix results of Ref. [20], the extended T-matrix results of Refs. [21, 54], and the Nozières and Schmitt-Rink (NSR) results of Ref. [55].

Several calculations found strong suppression of the spin susceptibility at temperatures above T_c (i.e., at $T/T_F \approx 0.25$ or higher) [15, 19, 20]. This was interpreted as evidence of a pseudogap or a spin gap. In our simulations, we find a suppression of χ_s only at much lower temperatures close to T_c (see also Fig. 9 of Ref. [33]). For the $13^3, N = 130$ system, χ_s is suppressed for $T \lesssim 0.17\,T_F$. We note, however, that χ_s is not fully converged to its thermodynamic limit in our calculations. Since for larger particle numbers, the suppression occurs at lower temperatures, we estimate an upper bound of $T^* \lesssim 0.17\,T_F$ for the spin-gap temperature at our filling factor of $\nu \simeq 0.06$. We also observe that our large-lattice results agree remarkably well with the theoretical results of Ref. [24].

(iv) Heat capacity: The heat capacity is difficult to compute in quantum Monte Carlo simulations due to large statistical fluctuations. To address this, we use the method of Ref. [63], in which the same set of auxiliary fields is used to compute the derivative $C_V = (\partial E/\partial T)_V$, greatly reducing the statistical errors. The heat capacity is shown in Fig. 2 for 20, 40, and 80 particles (solid symbols) along with the experimental results of Ref. [5] (open circles). We do not show the 130 particle results since the statistical errors are too large. We also show in Fig. 2 the NSR result of Ref. [64], the diagrammatic t-matrix result of Ref. [18], and the Luttinger-Ward results of Refs. [65, 66]. Our AFMC results are in overall agreement with the experimental results except for a shift in the peak to a lower temperature. For the $11^3, N = 80$ system the position of the peak at $T \simeq 0.135(10)T_F$ is consistent with the value of $T_c \simeq 0.130(15)T_F$ for our finite filling factor. We also note the overall agreement with the Luttinger-Ward results of Refs. [65, 66].

Ref. [64] described a significant enhancement of the UFG heat capacity at $T \gtrsim T_c$ relative to its value $C_V \approx 1$ in the BEC regime, and attributed this enhancement to metastable preformed cooper pairs present in a pseudogap regime. Similar enhancement was also observed in the t-matrix calculations of Ref. [18]. Our calculations confirm such an enhancement. As a function of temperature, we find that it washes out above $T \sim 0.17\,T_F$.

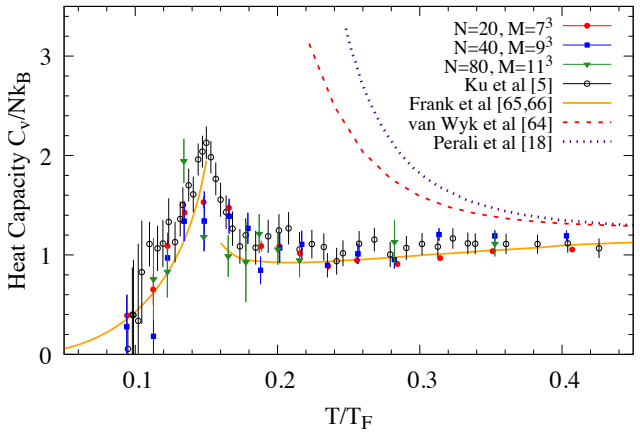

FIG. 2. The AFMC heat capacity (solid symbols) is compared to experiment [5] (open circles), the t-matrix result of Ref. [18] (dotted line), the NSR result of Ref. [64] (dashed line), and the Luttinger-Ward results of Refs. [65, 66] (solid lines).

Model space and spherical cutoff.— Signatures of a pseudogap were observed in the AFMC simulations of Refs. [13–15] for temperatures below $\sim 0.25\,T_F$. Those calculations used a single-particle model space with a spherical cutoff $|\mathbf{k}| \le k_c = \pi/\delta x$ in momentum. It was shown in Ref. [43] that when using such a cutoff, the inverse of the low-momentum scattering amplitude acquires a linear dependence on the center-of-mass momentum $\hbar\boldsymbol{K}$, and therefore this model does not reproduce the UFG even in the limit $k_F/k_c \to 0$. In Figs. 6-8 of Ref. [33] we demonstrate this effect in the scattering phase shifts and the two-particle energies. We also checked that our AFMC results change significantly when we introduce a spherical cutoff and become comparable to those of Refs. [13–15]; see Fig. 9 in Ref. [33].

Conclusion and outlook.— We have presented large-scale AFMC simulations of the homogeneous UFG at a small but finite filling factor of $\nu \simeq 0.06$. We calculated a model-independent pairing gap Δ_E, the condensate fraction, spin susceptibility, and heat capacity as a function of temperature, and compared these to experiments.

We find that Δ_E vanishes above the critical temperature T_c (which we determine to be $T_c \simeq 0.130(15)T_F$ for $\nu \simeq 0.06$), and thus does not show pseudogap effects. The spin susceptibility exhibits a moderate spin-gap effect in the range $T_c \lesssim T \lesssim 0.17\,T_F$ for our largest lattice used. This result is in contrast to previous AFMC calculations which claim spin-gap effects in a significantly wider range $T_c \lesssim T \lesssim 0.25\,T_F$ at similar filling factors.

Our conclusion holds for $\nu \simeq 0.06$. It still remains for future work to carry out the continuum extrapolation $\nu \to 0$ or equivalently $k_F r_e \to 0$.

Acknowledgments.— We thank G.F. Bertsch, T. Enss, N. Navon, and F. Werner for useful discussions. We also thank M.J.H. Ku for providing the experimental data of Ref. [5], and J. Carlson, J.E. Drut, T. Enss, B. Frank, P. Magierski, Y. Ohashi, P. Pieri, G. C. Strinati, H. Tajima, G. Wlazłowski, and W. Zwerger for providing theoretical results shown in Fig. 1 and Fig. 2 of the main text, and Fig. 4 of the supplemental material. This work was supported in part by the U.S. DOE grants Nos. DE-FG02-91ER40608, DE-SC0019521, and DE-FG02-00ER41132. The research presented here used resources of the National Energy Research Scientific Computing Center, which is supported by the Office of Science of the U.S. Department of Energy under Contract No. DE-AC02-05CH11231. We also thank the Yale Center for Research Computing for guidance and use of the research computing infrastructure.

[1] Y. Nishida and H. Abuki, Phys. Rev. D **72**, 096004 (2005).
[2] M. Randeria, Nature Physics **6**, 561 (2010).
[3] W. Ketterle and M. W. Zwierlein, Riv. Nuovo Cimento Soc. Ital. Fis. **31**, 247 (2008).
[4] B. Mukherjee, Z. Yan, P. B. Patel, Z. Hadzibabic, T. Yefsah, J. Struck, and M. W. Zwierlein, Phys. Rev. Lett. **118**, 123401 (2017).
[5] M. J. H. Ku, A. T. Sommer, L. W. Cheuk, and M. W. Zwierlein, Science **335**, 563 (2012).
[6] S. Nascimbene, N. Navon, K. Jiang, F. Chevy, and C. Salomon, Nature **463**, 1057 (2010).
[7] J. Kinast, A. Turlapov, J. E. Thomas, Q. Chen, J. Stajic, and K. Levin, Science **307**, 1296 (2005).
[8] A. Schirotzek, Y.-i. Shin, C. H. Schunck, and W. Ketterle, Phys. Rev. Lett. **101**, 140403 (2008).
[9] J. P. Gaebler, J. T. Stewart, T. E. Drake, D. S. Jin, A. Perali, P. Pieri, and G. C. Strinati, Nature Physics **6**, 569 (2010).
[10] D. Wulin, H. Guo, C.-C. Chien, and K. Levin, Phys. Rev. A **83**, 061601 (2011).
[11] S. Nascimbène, N. Navon, S. Pilati, F. Chevy, S. Giorgini, A. Georges, and C. Salomon, Phys. Rev. Lett. **106**, 215303 (2011).
[12] A. Sommer, M. Ku, G. Roati, and M. W. Zwierlein, Nature **472**, 201 (2011).
[13] P. Magierski, G. Wlazłowski, A. Bulgac, and J. E. Drut, Phys. Rev. Lett. **103**, 210403 (2009).
[14] P. Magierski, G. Wlazłowski, and A. Bulgac, Phys. Rev. Lett. **107**, 145304 (2011).
[15] G. Wlazłowski, P. Magierski, J. E. Drut, A. Bulgac, and K. J. Roche, Phys. Rev. Lett. **110**, 090401 (2013).
[16] C.-C. Chien, H. Guo, Y. He, and K. Levin, Phys. Rev. A **81**, 023622 (2010).
[17] C.-C. Chien and K. Levin, Phys. Rev. A **82**, 013603 (2010).
[18] A. Perali, F. Palestini, P. Pieri, G. C. Strinati, J. T. Stewart, J. P. Gaebler, T. E. Drake, and D. S. Jin, Phys. Rev. Lett. **106**, 060402 (2011).
[19] T. Kashimura, R. Watanabe, and Y. Ohashi, Phys. Rev. A **86**, 043622 (2012).
[20] F. Palestini, P. Pieri, and G. C. Strinati, Phys. Rev. Lett. **108**, 080401 (2012).
[21] H. Tajima, T. Kashimura, R. Hanai, R. Watanabe, and Y. Ohashi, Phys. Rev. A **89**, 033617 (2014).
[22] M. Pini, P. Pieri, and G. C. Strinati, Phys. Rev. B **99**, 094502 (2019).
[23] R. Haussmann, M. Punk, and W. Zwerger, Phys. Rev. A **80**, 063612 (2009).
[24] T. Enss and R. Haussmann, Phys. Rev. Lett. **109**, 195303 (2012).
[25] E. J. Mueller, Rep. Prog. Phys. **80**, 104401 (2017).
[26] W. Zwerger, *The BCS-BEC Crossover and the Unitary Fermi Gas* (Springer-Verlag, Heidelberg, 2012).
[27] E. Burovski, N. Prokof'ev, B. Svistunov, and M. Troyer, Phys. Rev. Lett. **96**, 160402 (2006).
[28] V. K. Akkineni, D. M. Ceperley, and N. Trivedi, Phys. Rev. B **76**, 165116 (2007).
[29] O. Goulko and M. Wingate, Phys. Rev. A **82**, 053621 (2010).
[30] J. E. Drut, T. A. Lähde, G. Wlazłowski, and P. Magierski, Phys. Rev. A **85**, 051601 (2012).
[31] K. Van Houcke, F. Werner, E. Kozik, N. Prokofev, B. Svistunov, M. Ku, A. Sommer, L. Cheuk, A. Schirotzek, and M. Zwierlein, Nature Physics **8**, 366 (2012).
[32] A. Bulgac, J. E. Drut, and P. Magierski, Phys. Rev. A **78**, 023625 (2008).
[33] See the Supplemental Material accompanying this article for additional details and for the data used to generate the figures. The supplemental text file cites additional Refs. [34–42].
[34] J. Carlson, S. Gandolfi, K. E. Schmidt, and S. Zhang, Phys. Rev. A **84**, 061602 (2011).
[35] M. G. Endres, D. B. Kaplan, J.-W. Lee, and A. N. Nicholson, Phys. Rev. A **87**, 023615 (2013).
[36] K. Binder, Phys. Rev. Lett. **47**, 693 (1981).
[37] R. Guida and J. Zinn-Justin, Journal of Physics A: Mathematical and General **31**, 8103 (1998).
[38] M. Campostrini, M. Hasenbusch, A. Pelissetto, and E. Vicari, Phys. Rev. B **74**, 144506 (2006).
[39] A. Pelissetto and E. Vicari, Physics Reports **368**, 549 (2002).
[40] E. Burovski, N. Prokof'ev, B. Svistunov, and M. Troyer, New Journal of Physics **8**, 153 (2006).
[41] L. Pricoupenko and Y. Castin, Journal of Physics A: Mathematical and Theoretical **40**, 12863 (2007).
[42] S. R. Beane, P. F. Bedaque, A. Parreo, and M. J. Savage, Physics Letters B **585**, 106 (2004).
[43] F. Werner and Y. Castin, Phys. Rev. A **86**, 013626 (2012).
[44] Y. Alhassid, "Auxiliary-field quantum monte carlo methods in nuclei," in *Emergent Phenomena in Atomic Nuclei from Large-Scale Modeling: a Symmetry-Guided Perspective*, edited by K. D. Launey (World Scientific, Singapore, 2017) pp. 267–298.
[45] R. L. Stratonovich, Dokl. Akad. Nauk SSSR [Sov. Phys. - Dokl.] **115**, 1097 (1957).
[46] J. Hubbard, Phys. Rev. Lett. **3**, 77 (1959).
[47] D. J. Dean, S. E. Koonin, G. H. Lang, P. B. Radha, and W. E. Ormand, Phys. Lett. B **317**, 275 (1993).
[48] C. N. Gilbreth and Y. Alhassid, Phys. Rev. A **88**, 063643 (2013).
[49] C. N. Gilbreth and Y. Alhassid, Computer Physics Communications **188**, 1 (2015).

[50] C. N. Gilbreth, S. Jensen, and Y. Alhassid, arXiv preprint arXiv:1907.10596 (2019).
[51] C. N. Yang, Rev. Mod. Phys. **34**, 694 (1962).
[52] S. Hoinka, P. Dyke, M. G. Lingham, J. J. Kinnunen, G. M. Bruun, and C. J. Vale, Nature Physics **13**, 943 (2017).
[53] J. Carlson and S. Reddy, Phys. Rev. Lett. **100**, 150403 (2008).
[54] H. Tajima, R. Hanai, and Y. Ohashi, Phys. Rev. A **93**, 013610 (2016).
[55] P.-A. Pantel, D. Davesne, and M. Urban, Phys. Rev. A **90**, 053629 (2014).
[56] M. M. Forbes, S. Gandolfi, and A. Gezerlis, Phys. Rev. A **86**, 053603 (2012).
[57] L. M. Schonenberg and G. J. Conduit, Phys. Rev. A **95**, 013633 (2017).
[58] A. Gezerlis and J. Carlson, Phys. Rev. C **77**, 032801 (2008).
[59] Y. Alhassid, S. Liu, and H. Nakada, Phys. Rev. Lett. **83**, 4265 (1999).
[60] J. Carlson, S.-Y. Chang, V. R. Pandharipande, and K. E. Schmidt, Phys. Rev. Lett. **91**, 050401 (2003).
[61] N. Trivedi and M. Randeria, Phys. Rev. Lett. **75**, 312 (1995).
[62] C. Huscroft, M. Jarrell, T. Maier, S. Moukouri, and A. N. Tahvildarzadeh, Phys. Rev. Lett. **86**, 139 (2001).
[63] S. Liu and Y. Alhassid, Phys. Rev. Lett. **87**, 022501 (2001).
[64] P. van Wyk, H. Tajima, R. Hanai, and Y. Ohashi, Phys. Rev. A **93**, 013621 (2016).
[65] W. Zwerger, "Strongly interacting fermi gases," in *Proceedings of the International School of Physics "Enrico Fermi" - Course 191 "Quantum Matter at Ultralow Temperatures"*, edited by M. Inguscio, W. Ketterle, S. Stringari, and G. Roati (IOS Press, Amsterdam, SIF Bologna, 2016) pp. 63–141.
[66] B. Frank, J. Lang, and W. Zwerger, JETP **127**, 812 (2018).